Meccanica (2015) 50:355–365
DOI 10.1007/s11012-014-0012-0

EXPERIMENTAL SOLID MECHANICS

Finite deformations of full sine-wave St.-Venant beam due to tangential and normal distributed loads using nonlinear TSNDT

R. C. Batra · J. Xiao

Received: 18 February 2014 / Accepted: 27 June 2014 / Published online: 24 July 2014

Abstract We analyze deformations of a beam initially in the form of a full sine wave and loaded by distributed tangential and normal surface tractions with the goal of finding how the beam curvature and the consideration of all nonlinearities affect the maximum values of stresses and deflections. The curvature of the beam in the left half is opposite of that in the right half of the beam, and the radius of curvature varies from point to point. The problem has been analyzed by using the third order shear and normal deformable beam theory (TSNDT) that accounts for all geometric nonlinearities. The beam material is St. Venant–Kirchhoff for which the second Piola–Kirchhoff stress tensor is a linear function of the Green–Lagrange strain tensor. It is found that for quasistatic deformation with non-dimensional pressure, $\bar{q}_0 = \frac{q_0 \mathbb{L}^4}{100 E_L H^4} = 2.6$, the axial stress at the point $\left(\frac{3\mathcal{L}}{4}, \frac{H}{2}\right)$ from the nonlinear theory equals nearly 4 times that from the linear theory. The lateral deflection at the point $\left(\frac{3\mathcal{L}}{4}, 0\right)$ from the nonlinear theory is about 1.5 times that from the linear theory. Here q_0 is the uniform pressure applied on the bottom surface of the beam, E_L Young's modulus in the longitudinal direction for infinitesimal deformations, H the beam height, $\mathbb{L}$ the horizontal distance between the two end faces, and $\mathcal{L}$ the arc length. Significant features of the work include using the TSNDT, accounting for all geometric nonlinearities, using a materially objective constitutive relation, considering curvature varying from positive to negative, and applying both tangential and normal surface tractions.

Keywords Sinusoidal beam · Geometric nonlinearities · Materially objective constitutive relation · Third-order shear and normal deformable beam theory

1 Introduction

Curved beams are often used as structural members. Various techniques to derive equations governing their deformations include the direct approach of Cosserat and Cosserat [1] in which directors are attached to every point of the curve passing through centroids of cross-sections of the beam. Deformations of directors account for in-plane deformations of a cross-section and the stretch along the curve gives the axial stretch of the beam. A challenge here is to derive appropriate constitutive relations and find values of material parameters. Alternatively, one can make kinematic assumptions on the displacement fields as is often

R. C. Batra (✉) · J. Xiao
Department of Engineering Science and Mechanics, M/C 0219, Virginia Polytechnic Institute and State University, Blacksburg, VA 24061, USA
e-mail: rbatra@vt.edu

J. Xiao
e-mail: xiaojian@vt.edu

done for the Euler–Bernoulli [2] and the Timoshenko [3] beam theories and derive equations for the beam from those of the three-dimensional elasticity theory. Classical works in this field also include those of Love [4], Reissener [5], Mindlin [6], and others. We refer the reader to Ericksen and Truesdell [7], Antman [8], Green and Naghdi [9] for the development of rod, beam, plate and shell theories. Chidamparam and Leissa [10], Hajiamaleki and Qatu [11], and Carrera and Petrolo [12] have reviewed the literature on beam theories wherein one can find additional references. Carrera and Petrolo [12] have also discussed ramifications of including terms of various order in a beam theory.

Lo et al. [13], Vidoli and Batra [14], as well as Batra and Vidoli [15, 16] followed Mindlin's approach of expanding displacement components in terms of the thickness coordinate z and retaining terms up to various order in z. Governing equations for the kinematic variables and the constitutive relations for the kinetic variables are usually derived by taking moments about the centroidal axis of the beam of the three-dimensional equations of motion and the constitutive relations, and integrating these over the beam thickness.

For finite deformations of these structural members it is common to include in the strain–displacement relations only nonlinear terms in the gradients of the transverse deflection proposed by von Karman and neglect transverse normal strains. These approximations pose the challenge of either adopting an appropriate materially objective constitutive relation or delineating approximations made in the constitutive relation. The authors are not aware of a stress tensor that is work conjugate to the strain tensor that does not include all nonlinear terms in displacement gradients. Of course, the error introduced in the solution of a problem by not using a materially objective constitutive relation depends upon loads, initial and boundary conditions, and magnitudes of rotations and strains. The error can only be quantified when a solution of the nonlinear problem using a materially objective constitutive relation is available.

Allix and Corigliano [17] used kinematic assumptions for the Timoshenko beam theory, derived expressions for the Green-St. Venant strain tensor, and used the St. Venant–Kirchhoff material for the beam to study delamination in a double cantilever beam. For a body stress free in the reference configuration and made of the St. Venant–Kirchhoff material, the second Piola–Kirchhoff stress tensor is a linear function of the Green-St. Venant strain tensor, and the strain energy density per unit reference volume is a quadratic function of the Green-St. Venant strain tensor. This constitutive relation is materially objective since both the second Piola–Kirchhoff stress tensor and the Green-St. Venant strain tensors transform as scalars under a rigid body motion superimposed upon the present configuration of the body. Batra [23] has shown that the response predicted by four linear materially objective constitutive relations that give identical results for infinitesimal deformations yield totally different results for finite deformations.

Batra and Xiao [18–20] adopted a third order shear and normal deformable beam theory (TSNDT) in which the two in-plane displacement components are expanded up to third-order terms in the thickness coordinate z, kept all nonlinear terms in the Green-St. Venant strain tensor, and used the St. Venant–Kirchhoff material for the beam. They used this beam theory to study delamination in straight and curved laminated beams, and also hydroelastic fluid–structure interaction during entry into water of a sandwich beam. Here we use this theory to analyze the effect of geometric nonlinearities on a curved beam that in the undeformed stress-free configuration is in the form of a full sine wave. One of the goals is to identify the cross-section on which stresses are the maximum. We note that there is no shear correction factor used in this theory, and transverse shear and transverse normal stresses are found from the displacement field rather than through a stress recovery scheme in which in-plane stresses are found from the computed displacement field and the transverse normal and the transverse shear stresses by integrating with respect to z the equilibrium equations, e.g., see [21].

2 Problem formulation

2.1 Kinematics

A schematic sketch of the problem studied is shown in Fig. 1 in which y_1, y_2, y_3 are orthogonal curvilinear coordinate axes in the reference configuration with y_1-axis along the tangent to the mid-surface of the beam, y_2-axis pointing into the plane of the paper, and y_3-axis

Fig. 1 Schematic sketch of a curved beam

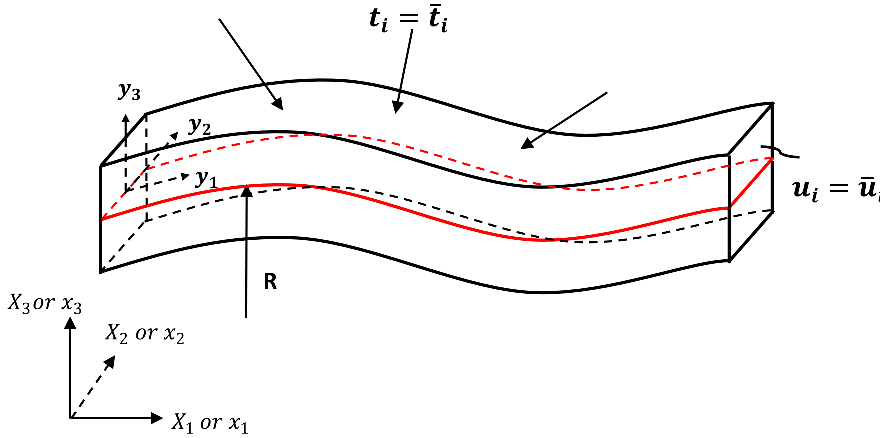

pointing along the local thickness direction. Furthermore, X_1, X_2, X_3 and x_1, x_2, x_3 are fixed rectangular Cartesian coordinate axes with the y_2-axis parallel to the x_2- and the X_2- axes. Let position vectors, with respect to the fixed rectangular Cartesian coordinate axes, of a point p located at (y_1, y_2, y_3) in the reference configuration be $\boldsymbol{x}$ and $\boldsymbol{X}$ in the current and the reference configurations, respectively. The displacement $\boldsymbol{u}$ of point p and components, G_{ij}, of the metric tensor in the reference configuration are given by

$$\boldsymbol{u} = \boldsymbol{x} - \boldsymbol{X} \tag{1}$$

$$G_{ij} = \boldsymbol{A}_i \cdot \boldsymbol{A}_j,\ \boldsymbol{A}_i = \frac{\partial \boldsymbol{X}}{\partial y_i} \tag{2}$$

For orthogonal curvilinear coordinate axes G_{ij} is non-zero only when $i = j$. We set

$$H_1 = \sqrt{G_{11}},\ H_2 = \sqrt{G_{22}} = 1,\ H_3 = \sqrt{G_{33}} = 1,\ \tilde{e}_j = \frac{\boldsymbol{A}_i}{H_{(i)}} (\text{no sum on}\ i) \tag{3}$$

Here $(\tilde{e}_1, \tilde{e}_2, \tilde{e}_3)$ are unit base vectors for the curvilinear coordinate axes in the reference configuration. We note that

$$H_1 = \left(1 + \frac{y_3}{R}\right),\ \frac{\partial \tilde{e}_1}{\partial y_1} = -\frac{\tilde{e}_3}{R},\ \frac{\partial \tilde{e}_3}{\partial y_1} = \frac{\tilde{e}_1}{R} \tag{4}$$

where R is the radius of curvature at the point (y_1, y_2, y_3).

Physical components of the deformation gradient, $\boldsymbol{F}$, and the Green-St. Venant strain tensor, $\boldsymbol{E} = \frac{1}{2}\left(\boldsymbol{F}^T\boldsymbol{F} - \mathbf{1}\right)$, with $\mathbf{1}$ being the identity tensor are given by

$$[F] = \begin{bmatrix} 1 + \frac{1}{H_1}\left(\frac{\partial u_1}{\partial y_1} + \frac{u_3}{R}\right) & 0 & \frac{\partial u_1}{\partial y_3} \\ 0 & 1 & 0 \\ \frac{1}{H_1}\left(\frac{\partial u_3}{\partial y_1} - \frac{u_1}{R}\right) & 0 & 1 + \frac{\partial u_3}{\partial y_3} \end{bmatrix} \tag{5.a}$$

$$\begin{aligned} E_{11} &= \frac{1}{H_1}\left(\frac{\partial u_1}{\partial y_1} + \frac{u_3}{R}\right) + \frac{1}{2H_1^2}\left[\left(\frac{\partial u_1}{\partial y_1} + \frac{u_3}{R}\right)^2 + \left(\frac{\partial u_3}{\partial y_1} - \frac{u_1}{R}\right)^2\right] \\ E_{33} &= \frac{\partial u_3}{\partial y_3} + \frac{1}{2}\left[\left(\frac{\partial u_1}{\partial y_3}\right)^2 + \left(\frac{\partial u_3}{\partial y_3}\right)^2\right] \\ 2E_{13} &= \frac{1}{H_1}\left(\frac{\partial u_3}{\partial y_1} - \frac{u_1}{R}\right) + \frac{\partial u_1}{\partial y_3} + \frac{1}{H_1}\left[\frac{\partial u_3}{\partial y_3}\left(\frac{\partial u_3}{\partial y_1} - \frac{u_1}{R}\right) + \frac{\partial u_1}{\partial y_3}\left(\frac{\partial u_1}{\partial y_1} + \frac{u_3}{R}\right)\right] \end{aligned} \tag{5.b}$$

We note that $\boldsymbol{E}$ incorporates all geometric nonlinearities including the von Kármán nonlinearity, and is valid for finite (or large) deformations of a beam. The strain tensor for infinitesimal deformations is obtained from Eq. (5) by neglecting the nonlinear terms included in brackets. When only the von Kármán nonlinearities are considered, we get

$$\begin{aligned} E_{11} &= \frac{1}{H_1}\left(\frac{\partial u_1}{\partial y_1} + \frac{u_3}{R}\right) + \frac{1}{2H_1^2}\left(\frac{\partial u_3}{\partial y_1}\right)^2 \\ E_{33} &= \frac{\partial u_3}{\partial y_3} \\ 2E_{13} &= \frac{1}{H_1}\left(\frac{\partial u_3}{\partial y_1} - \frac{u_1}{R}\right) + \frac{\partial u_1}{\partial y_3} \end{aligned} \tag{6}$$

Recalling that beam's dimension along the y_3- (or the z-) axis is considerably smaller than that along the y_1-axis, we assume the following third order Taylor series expansion in y_3 for u_1 and u_3:

$$u_1(y_1, y_3, t) = \sum_{i=0}^{3} (y_3)^i u_{1i}(y_1, t) = L_i(y_3) u_{1i}(y_1, t) \tag{7.a}$$

$$u_3(y_1, y_3, t) = L_i(y_3) u_{3i}(y_1, t) \tag{7.b}$$

$$\begin{aligned} &L_j(y_3) = (y_3)^j, \\ &L_j^{'}(y_3) = \mathrm{D_{ji}} L_i(y_3) \text{ (summed on } i; i, j = 0, 1, 2, 3) \end{aligned} \tag{7.c, d}$$

$$[\mathrm{D}] = \begin{bmatrix} 0 & 0 & 0 & 0 \\ 1 & 0 & 0 & 0 \\ 0 & 2 & 0 & 0 \\ 0 & 0 & 3 & 0 \end{bmatrix} \tag{7.e}$$

Here and below a repeated index implies summation over the range of the index. In Eq. (7), u_{10} and u_{30} are, respectively, the axial and the transverse displacements of a point on the beam mid-surface, u_{1i} and $u_{3i}(i = 1, 2, 3)$ may be interpreted as generalized axial and transverse displacements of a point, $L_j^{'}(y_3)$ equals the derivative of $L_j(y_3)$ with respect to y_3, and t denotes the time. The first subscript on u corresponds to the displacement direction, and the second subscript to the power of y_3. For $u_{10} = u_{12} = u_{13} = u_{31} = u_{32} = u_{33} = 0$, we get the Timoshenko beam theory, and when $u_{11} = -\frac{\partial u_{30}}{\partial y_1}$ the Euler–Bernoulli beam theory. The displacement field in Eq. (7) is a special case of the Kth order displacement field considered amongst others, by Batra and Vidoli [14], Carerra and Petrolo [12], Lo et al. [13], and Cho et al. [22]. We call the beam theory based on Eq. (7) the TSNDT. Note that it accounts for the transverse normal strain and does not assume the transverse shear strain at the top and the bottom surfaces to be zero. Substitution for u_1 and u_3 from Eq. (7) into Eqs. (5) and (6) gives expressions for physical components of the deformation gradient $\boldsymbol{F}$ and the Green-St. Venant strain tensor $\boldsymbol{E}$.

2.2 Kinetics

The in-plane displacements (u_1, u_3) of a point are governed by the following equations expressing the balance of linear momentum written in the Lagrangian description of motion using physical components $T_{11}, T_{13}, T_{31}, T_{33}$, of the first Piola–Kirchhoff stress tensor [6], and initial and boundary conditions.

$$\rho_0\, \ddot{u}_1 = \frac{1}{H_1}\frac{\partial T_{11}}{\partial y_1} + \frac{1}{H_1}\frac{\partial (H_1 T_{13})}{\partial y_3} + \frac{1}{H_1 R} T_{31} + f_1 \tag{8.a}$$

$$\rho_0\, \ddot{u}_3 = \frac{1}{H_1}\frac{\partial T_{31}}{\partial y_1} + \frac{1}{H_1}\frac{\partial (H_1 T_{33})}{\partial y_3} - \frac{1}{H_1 R} T_{11} + f_3 \tag{8.b}$$

$$u_i(y_1, y_3, 0) = u_i^0(y_1, y_3), \dot{u}_i(y_1, y_3, 0) = \dot{u}_i^0(y_1, y_3) \tag{8.c, d}$$

$$\begin{aligned} &T_{ij} N_j = \bar{t}_j(y_1, y_3, t) \text{ on } \Gamma_{\mathrm{t}}, \\ &u_i(y_1, y_3, t) = \bar{u}_i(y_1, y_3, t) \text{ on } \Gamma_{\mathrm{u}},\ i, j = 1 \text{ and } 3 \end{aligned} \tag{8.e, f}$$

In Eq. (8) f_1 and f_3 are components of the body force per unit reference volume along the y_1- and the y_3-axes, respectively, ρ_0 is the mass density in the reference configuration, and $\ddot{u}_i = \frac{\partial^2 u_i}{\partial t^2}$. The initial displacement u_i^0 and the initial velocity $\dot{u}_i^0$ are known functions of y_1 and y_3. Furthermore, $\boldsymbol{N}$ is a unit outward normal in the reference configuration at a point on the boundary Γ_{t} where surface tractions are prescribed as $\bar{t}_i$. On the remaining boundary, Γ_{u}, displacements are prescribed as $\bar{u}_i$.

We multiply both sides of Eqs. (8.a) and (8.b) with $L_j(y_3)$, $j = 0, 1, 2, 3$, and integrate the resulting equations over the beam thickness to obtain the following.

$$A_{ji}\, \ddot{u}_{1i} = \frac{\partial M_{11}^j}{\partial y_1} - D_{ji} M_{13}^i + \frac{1}{R} M_{31}^j + \bar{f}_1^j + B_{13}^j, \quad j, i = 0, 1, 2, 3 \tag{9.a}$$

$$A_{ji}\, \ddot{u}_{3i} = \frac{\partial M_{31}^j}{\partial y_1} - D_{ji} M_{33}^i - \frac{1}{R} M_{11}^j + \bar{f}_3^j + B_{33}^j, \quad j, i = 0, 1, 2, 3 \tag{9.b}$$

Here

$$M_{mn}^j(y_1, t) = \int_{-\mathrm{H}/2}^{\mathrm{H}/2} L_j(y_3) T_{mn} \mathcal{H}_{(n)} dy_3,\ \mathcal{H}_{(1)} = 1, \quad \mathcal{H}_{(3)} = H_1 \tag{10.a}$$

$$B_{13}^{j}(y_1,t) = L_j(H/2)H_1T_{13}(H/2,t) - L_j(-H/2)H_1T_{13}(-H/2,t) \quad (10.b)$$

$$B_{33}^{j}(y_1,t) = L_j(H/2)H_1T_{33}(H/2,t) - L_j(-H/2)H_1T_{33}(-H/2,t) \quad (10.c)$$

$$\bar{f}_{\alpha}^{j}(y_1,t) = \int_{-\mathrm{H}/2}^{\mathrm{H}/2} L_j(y_3)f_{\alpha}H_1dy_3 \quad (10.d)$$

$$A_{ji}(y_1,t) = \int_{-\frac{H}{2}}^{\frac{H}{2}} L_j(y_3)L_i(y_3)\rho_0H_1dy_3, \quad (10.e)$$

$m,n,\alpha = 1,3,$ and $i,j = 0,1,2,3.$

The quantity M_{mm}^{j} equals jth order moment of the stress T_{mn} about the y_2-axis; M_{mm}^{0} is usually called the resultant force, and M_{mm}^{1} the bending moment. The quantities B_{13}^{j} and B_{33}^{j} equal jth order moments about the y_2-axis of the tangential surface traction T_{13} and the normal surface traction T_{33} applied on the top and the bottom surfaces of the beam; for $j = 0$ these equal the resultant forces and for $j = 1$ their first-order moments about the y_2-axis. Similarly, $\bar{f}_{\alpha}^{j}$ equals jth order moment of the body force f_{α} about the y_2-axis, and A_{ji} the inertia tensor associated with the generalized displacements u_{1i} and u_{3i}.

After expressions for moments M_{mn}^{j} in terms of displacements have been substituted in Eq. (8), we obtain governing equations of motion for the curved beam which are 8 nonlinear coupled partial differential equations (PDEs) for the 8 unknowns, u_{1j} and u_{3j}. These PDEs involve second-order derivatives of u_{1j} and u_{3j} with respect to y_1 and time t and are to be solved under pertinent initial and boundary conditions.

The traction boundary conditions in Eq. (8.e) on the top and the bottom surfaces of the beam are incorporated in Eq. (9); e.g., see Eqs. (10.b) and (10.c). Eight boundary conditions at a clamped, simply supported and traction free edge, say $y_1 = 0$, respectively, are

$$u_{\alpha j}(0,t) = 0, \quad \alpha = 1,3,\ j = 0,1,2,3, \quad (11.a)$$

$$u_{3j}(0,t) = 0,\ M_{11}^{j}(0,t) = 0, \quad (11.b)$$

$$M_{11}^{j}(0,t) = 0, M_{31}^{j}(0,t) = 0. \quad (11.c)$$

In order to derive initial conditions, we substitute from Eq. (7) into Eqs. (8.c) and (8.d), multiply both sides of the resulting equations with $\rho_0L_j(y_3)$, and integrate with respect to y_3 on the domain $(-\mathrm{H}/2, \mathrm{H}/2)$ to obtain the following equations from which initial values $u_{\alpha i}(y_1, 0)$ and $\dot{u}_{\alpha i}(y_1,0)$ are determined.

$$A_{ji}u_{\alpha i}(y_1,0) = \int_{-\mathrm{H}/2}^{\mathrm{H}/2} \rho_0L_j(y_3)u_{\alpha}^{0}(y_1,y_3)dy_3 = \mathcal{F}_{\alpha j}(y_1) \quad (12.a)$$

$$A_{ji}\dot{u}_{\alpha i}(y_1,0) = \int_{-\mathrm{H}/2}^{\mathrm{H}/2} \rho_0L_j(y_3)\dot{u}_{\alpha}^{0}(y_1,y_3)dy_3 = \dot{\mathcal{F}}_{\alpha j}(y_1), \alpha = 1,3; i,j = 0,1,2,3 \quad (12.b)$$

Even though the equations governing transient deformations of the beam have been developed, results for only static problems are presented here.

2.3 Constitutive relations

We assume that the beam material is St. Venant–Kirchhoff for which the strain energy density, W, per unit reference volume is given by

$$S_{mn} = \frac{\partial W}{\partial E_{mn}}, W = \frac{1}{2}E_{mn}C_{mn\alpha\beta}E_{\alpha\beta}, \quad C_{mn\alpha\beta} = C_{\alpha\beta mn} = C_{nm\alpha\beta} \quad (13)$$

Here $\boldsymbol{C}$ is the fourth-order elasticity tensor having 21 independent components for a general anisotropic material. The independent components of $\boldsymbol{C}$ reduce to 9, 5 and 2 for an orthotropic, transversely isotropic and isotropic material, respectively. The strain energy density for the St. Venant–Kirchhoff material reduces to that of a Hookean material if the finite strain tensor $\boldsymbol{E}$ in Eq. (13) is replaced by the infinitesimal deformations strain tensor $e_{\alpha\beta}$.

For plane strain deformations of an orthotropic material with the material principal axes coincident with the coordinate axes (y_1, y_2, y_3), Eq. (13) reduces to

$$\begin{Bmatrix} S_{11} \\ S_{33} \\ S_{13} \end{Bmatrix} = \begin{bmatrix} C_{1111} & C_{1133} & 0 \\ C_{3311} & C_{3333} & 0 \\ 0 & 0 & C_{1313} \end{bmatrix} \begin{Bmatrix} E_{11} \\ E_{33} \\ 2E_{13} \end{Bmatrix} \quad (14)$$

Recalling that $\boldsymbol{T} = \boldsymbol{FS}$, where $\boldsymbol{T}$ is the first Piola–Kirchhoff stress tensor, we get

$$\begin{bmatrix} T_{11} & T_{13} \\ T_{31} & T_{33} \end{bmatrix} = \begin{bmatrix} F_{11}S_{11} + F_{13}S_{13} & F_{11}S_{13} + F_{13}S_{33} \\ F_{31}S_{11} + F_{33}S_{13} & F_{31}S_{13} + F_{33}S_{33} \end{bmatrix} \tag{15}$$

Substitution for $\boldsymbol{F}$ from Eq. (5) into Eq. (15), and for $\boldsymbol{E}$ from Eq. (6) into Eq. (14) and the result into Eq. (15) gives expressions for $\boldsymbol{T}$ in terms of generalized displacements u_{1i} and u_{3i} and four elastic constants C_{1111}, C_{1133}, C_{3333}, and C_{1313}. Even though components of $\boldsymbol{S}$ are quadratic in displacement gradients those of $\boldsymbol{T}$ are cubic in displacement gradients. Thus constitutive relation (15) accounts for material nonlinearities in the sense that components of $\boldsymbol{T}$ are nonlinear functions of displacement gradients. We note that constitutive relations (13), (14) and (15) are materially objective and are invariant under a rigid body motion superimposed upon the present configuration. The true stress or the Cauchy stress, $\boldsymbol{\sigma}$, is related to the first Piola–Kirchhoff stress by $\boldsymbol{\sigma} = \frac{1}{J}\boldsymbol{T}\boldsymbol{F}^T$, where J is the determinant of the deformation gradient $\boldsymbol{F}$. Thus components of $\boldsymbol{\sigma}$ are complicated functions of displacement gradients because of the appearance of J in the denominator in the expression for $\boldsymbol{\sigma}$.

3 Problem solution

We are unable to analytically solve the above formulated nonlinear problem; thus we analyze it numerically. We refer the reader to Ref. [18] for derivations of the weak, the Galerkin and the matrix formulations of the problem, and verification of the developed computer code by the method of manufactured solutions. Here we present below results for static deformations of a sinusoidal curved beam under different loads. We assume that the material principal axes coincide with the coordinate axes shown in Fig. 2 and the beam is loaded by a uniformly distributed surface traction, q_0, on the bottom surface that makes angle θ, in the reference configuration, with the tangent to the beam centroidal axis. In fig. 2 we have used (x, z) for the axes (y_1, y_3). For $\theta = 0°$, $30°$ and $90°$, the surface tractions are tangential, mixed and normal to the beam surface in the reference configuration. Values of material parameters for the beam are listed below.

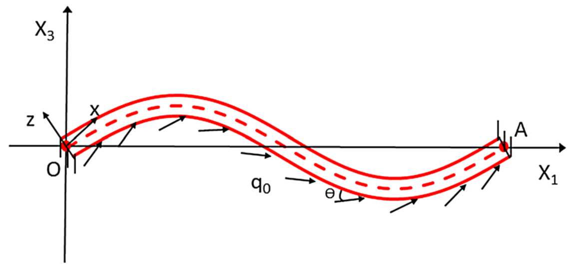

Fig. 2 Schematic sketch of a clamped–clamped full sine-wave beam loaded by uniformly distributed surface traction, q_0, on the bottom surface that makes angle θ with the tangent to the beam centroidal axis

$$E_L = 172\ GPa, E_T = 6.9\ GPa, G_{LT} = 3.4\ GPa,$$
$$G_{TT} = 1.4\ GPa, \nu_{TL} = \nu_{TT} = 0.25 \tag{16}$$

Here subscript L denotes the direction parallel to the fiber or the x-axis, subscript T the transverse direction or the z-axis, ν is Poisson's ratio, and G_{LT} is the shear modulus in the x z-plane.

The beam centroidal axis in the reference configuration is assumed to be described by

$$X_3 = \alpha\mathbb{L} * sin\left(\frac{2\pi X_1}{\mathbb{L}}\right), \quad X_1 \in [0, \mathbb{L}] \tag{17}$$

where $\mathbb{L} = 25.4$ cm is the X_1-coordinate of point A in Fig. 2, the beam thickness, $H = 1.27$ cm, the non-dimensional parameter $\alpha = 0.1$ defines the amplitude of sine wave, i.e., of the beam centroidal axis. Thus the curvature of the beam for $X_1 \in \left[0, \frac{\mathbb{L}}{2}\right]$ is opposite of that for $X_1 \in [\mathbb{L}/2, \mathbb{L}]$. Below we use the more common notation $(u,\ w)$ for the axial and the lateral displacements.

The deflection, w, along the z-axis, is normalized by

$$\bar{w} = \frac{100E_1H^3w}{q_0\mathbb{L}^4} \tag{18}$$

The centroidal axis is divided into uniform 2-node elements, thus piecewise linear basis functions are used to compute results with the TSNDT. For N nodes along the beam axis, the total number of degrees of freedom equal 8 N. If plane strain deformations of the beam were analyzed using 4-node quadrilateral elements, (N − 1) elements

Table 1 Stresses and deflections at critical points (indicated by coordinates (x, z)) from the linear theory for the sinusoidal beam loaded by uniformly distributed tractions with θ = 0°, 30° and 90° on the bottom surface of the beam

θ	Number of elements	$\sigma_{xx}/q_0\ \left(\frac{\mathcal{L}}{2}, \frac{H}{2}\right)$	$\sigma_{xx}/q_0\ \left(\frac{\mathcal{L}}{2}, -\frac{H}{2}\right)$	$\sigma_{xz}/q_0\ \left(\frac{3\mathcal{L}}{4}, 0\right)$	$\sigma_{zz}/q_0\ \left(\frac{3\mathcal{L}}{4}, -\frac{H}{2}\right)$	$\sigma_{xz}/q_0\ \left(\frac{3\mathcal{L}}{4}, -\frac{H}{2}\right)$	$\bar{w}\left(\frac{\mathcal{L}}{2}, 0\right)$
0°	81	−39.61	40.46	2.507	−0.00351	−1.013	−0.1924
	121	−39.61	40.46	2.507	−0.00323	−1.013	−0.1924
30°	81	21.24	−20.96	−1.524	−0.8733	−0.5013	0.0448
	121	21.24	−20.96	−1.525	−0.8733	−0.5013	0.0448
90°	81	−111.1	−112.0	−7.390	−0.9965	0.00850	0.4229
	121	−111.1	−112.0	−7.391	−0.9971	0.00872	0.4229

along the beam axis and 3 elements through the beam thickness, we will have 8N degrees of freedom. The FE mesh is successively refined to obtain a converged solution of the problem.

3.1 Results from the linear theory

For 81 and 121 uniform 2-node FEs along the beam centroidal axis, we have listed in Table 1 stresses and deflections at critical points from the linear theory for the beam loaded by uniformly distributed tractions with $\theta = 0^\circ$, 30° and 90° on the bottom surface of the beam. Here, $\mathcal{L} = 27.8$ cm equals the beam length along the centroidal axis. We note that for $\theta = 0^\circ$ and 90° the applied tractions are, respectively, tangent and normal to the bottom surface of the beam where surface tractions are applied. For $\theta = 30^\circ$ the applied surface tractions have both tangential and normal components. The differences in stresses and the deflection computed by the two FE meshes at critical points listed in Table 1 are small implying that the solution has converged. The traction boundary conditions on the bottom surface of the beam are also well satisfied. For $\theta = 30^\circ$ differences in the applied and the computed values of the shear traction, σ_{xz}, and the normal traction, σ_{zz}, on the bottom surface are 0.2 % and 0.8 %, respectively. For $\theta = 0^\circ$ and 90°, differences in the applied and the computed values of the tangential tractions on the bottom surface equal 1 % and 0.3 %, respectively.

For $\theta = 0^\circ, 30^\circ$ and 90° we have exhibited in Fig. 3 through-the-thickness distributions of the axial, the transverse shear and the transverse normal stresses on the section $x = 3\mathcal{L}/4$. Because of the curvature of the beam, σ_{xx} does not vanish at the mid-surface, z = 0, the variation of σ_{xx} with z is non-linear, and the distributions of σ_{xx} and σ_{zz} are not symmetric about the mid-surface.

In Fig. 4 we have plotted the variation of the transverse normal stress and the transverse shear stress on the bottom and the mid-surfaces of the beam, respectively. For the bottom surface loaded by normal pressure, the curvature of the beam results in positive and negative values of the axial stress on beam's bottom surface with the axial stress being positive near the edges and compressive in the middle of the beam. However, the axial stress is of opposite sign in these regions for the tangential traction applied on beam's bottom surface. The effect of axial variation in beam's curvature is more evident in distributions of the transverse normal and the transverse shear stresses.

The effect of curvature on beam's deformations has been studied by changing the value of α in Eq. (17). Let $R = \mathbb{L}/(4\pi^2\alpha)$ denote the minimum absolute radius of curvature of the beam. Thus for $\alpha = 0.1$, 0.05 and 0, R equals 6.43, 12.9 and ∞ cm, respectively. We note that $\alpha = 0$ corresponds to a straight beam. For these three values of R and $\theta = 90^\circ$, we have plotted in Fig. 5a–c the variation of the axial stress on the bottom surface, of the transverse shear stress on the mid-surface and the normalized deflected shape of the mid-surface of the beam. Values of R do not significantly affect the distribution of the axial stress on the bottom surface, and influence the transverse shear stress on the mid surface only at points near the two clamped edges. However, results plotted in Fig. 5c suggest that the deflection of the point ($\mathcal{L}/2$, 0) increases with an increase in the value of R. The increase in the centroidal deflection is considerably more when R is increased from 6.43 to 12.9 cm than when it is increased from 12.9 cm to ∞. The mid-span deflection for R = 6.43 cm is 15 % less

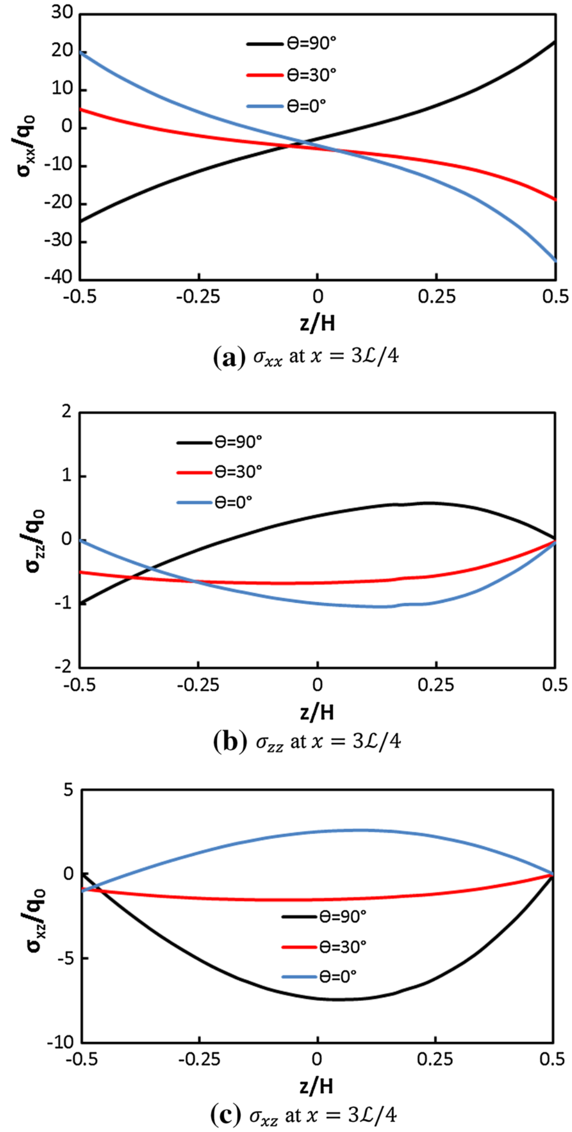

(a) σ_{xx} at $x = 3\mathcal{L}/4$

(b) σ_{zz} at $x = 3\mathcal{L}/4$

(c) σ_{xz} at $x = 3\mathcal{L}/4$

Fig. 3 Through-the-thickness distributions of stresses from the linear theory for the beam loaded by uniformly distributed tractions with $\theta = 0°$, 30° and 90° on the bottom surface of the beam (121 elements)

than that of the straight beam (R $= \infty$). The slope at the clamped edges does not appear to be zero as is assumed in the Euler–Bernoulli beam theory.

3.2 Results from the non-linear theory

We set $\alpha = 0.1$, and consider uniformly distributed pressure acting on the bottom surface of the beam in the current or the deformed configuration. The pressure is normalized by

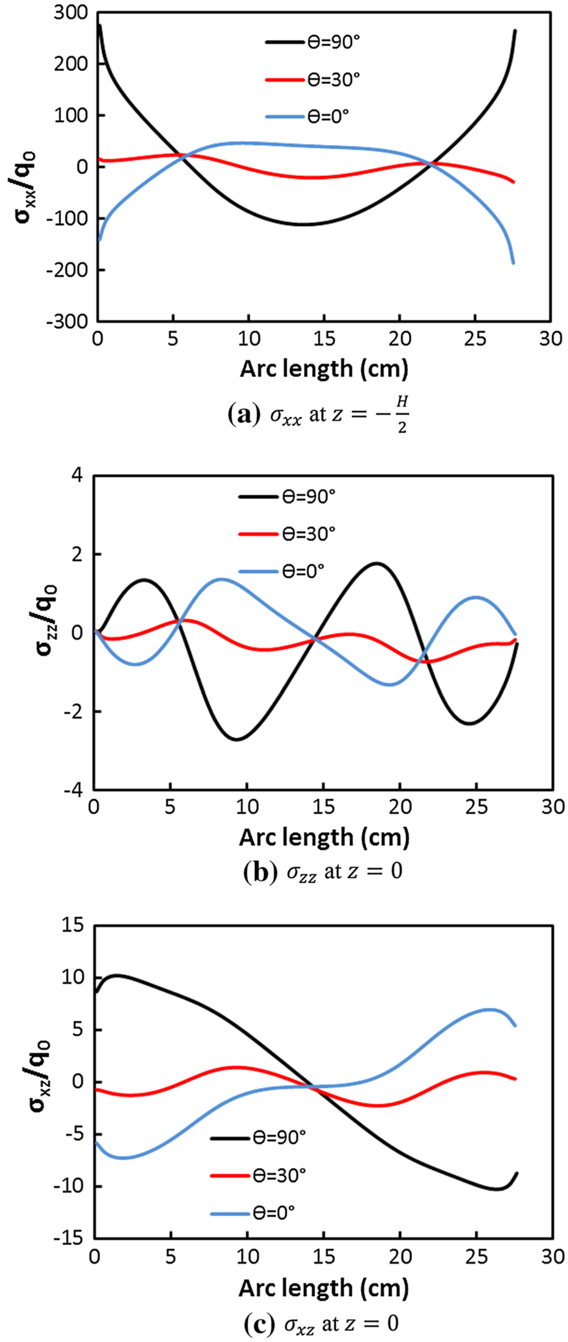

(a) σ_{xx} at $z = -\frac{H}{2}$

(b) σ_{zz} at $z = 0$

(c) σ_{xz} at $z = 0$

Fig. 4 Distributions of the axial stress, the transverse normal stress and the transverse shear stress on the bottom and the mid-surfaces of the beam from the linear theory for the beam loaded by uniformly distributed surface tractions with $\theta = 0°$, 30° and 90° on the bottom surface of the beam (121 elements)

$$\bar{q}_0 = \frac{q_0 \mathbb{L}^4}{100 E_L H^4} \tag{19}$$

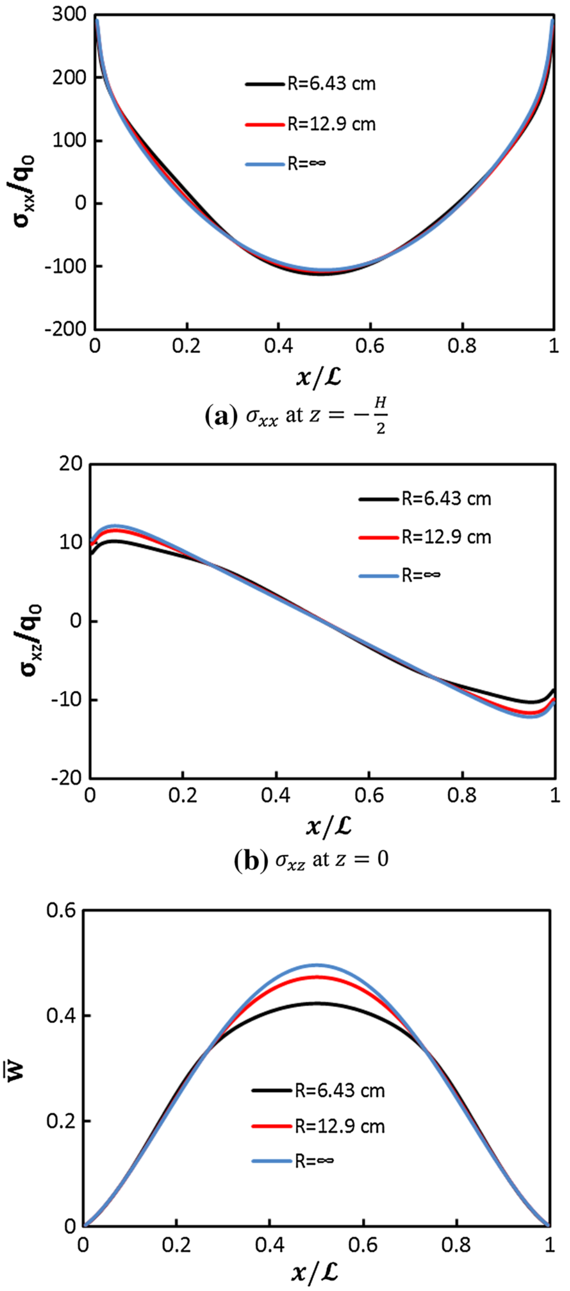

(a) σ_{xx} at $z = -\frac{H}{2}$

(b) σ_{xz} at $z = 0$

(c) $\overline{w}$ at $z = 0$

Fig. 5 For R = 6.43, 12.9 and ∞ cm, distributions of the axial stress on the bottom surface, the transverse shear stress on the mid-surface, and the transverse deflection of the mid-surface for the beam loaded by uniformly distributed tractions with $\theta = 90°$ on the bottom surface of the beam (121 elements)

and results presented below are for $\bar{q}_0 = 2.56$. The influence of the von Kármán geometric nonlinearity has been studied by assuming the 2nd Piola–Kirchhoff stress tensor is a linear function of the von Kármán strain.The material defined by this constitutive relation is not hyperelastic since the second Piola–Kirchhoff stress tensor cannot be obtained by differentiating the strain energy density with respect to the von Kármán strain tensor. We have listed in Table 2 the normalized axial stress, the normalized transverse shear stress and the normalized deflection at some points of the beam. These results suggest that the axial stress at points $\left(\frac{3\mathcal{L}}{4}, -\frac{H}{2}\right)$ and $\left(\frac{3\mathcal{L}}{4}, \frac{H}{2}\right)$ from the nonlinear theory equal 3.15 and 3.87 times that from the linear theory. The deflection at the point $\left(\frac{3\mathcal{L}}{4}, 0\right)$ computed using the nonlinear theory equals 1.48 times that from the linear theory. Thus results from the two theories are quite different. The results considering von Kármán geometric nonlinearities are between those of the linear and the nonlinear theories.

Table 2 Stresses and deflection at critical points from the linear and the nonlinear theories for the beam loaded by a uniformly distributed normal pressure on the bottom surface of the beam and non-dimensional pressure $\bar{q}_0 = 2.56$ (121 elements)

	σ_{xx}/q_0 $\left(\frac{3\mathcal{L}}{4}, -\frac{H}{2}\right)$	σ_{xx}/q_0 $\left(\frac{3\mathcal{L}}{4}, \frac{H}{2}\right)$	σ_{xz}/q_0 $\left(\frac{3\mathcal{L}}{4}, 0\right)$	w/H $\left(\frac{3\mathcal{L}}{4}, 0\right)$
Linear	−24.68	22.90	−7.39	0.83
Nonlinear	−77.68	88.70	−5.07	1.23
Nonlinear (von Kármán)	−52.18	62.55	−6.81	1.01

For the linear and the nonlinear theories, we have plotted in Fig. 6 the non-dimensional deflection of the point $(3\mathcal{L}/4, 0)$ versus the non-dimensional pressure $\bar{q}_0$. It is clear that the consideration of geometric and material nonlinearities increases the deflection of the point $(3\mathcal{L}/4, 0)$ and the difference in deflections from the two theories increases with an increase in the value of $\bar{q}_0$ and becomes noticeable for $\bar{q}_0 > 2$ even though effects of nonlinearities begin to show for $\bar{q}_0 = 1.5$. The difference between full nonlinearities and considering von Kármán geometric nonlinearity only will become significant for $\bar{q}_0 > 2.4$.

The computed deformed shapes of the mid-surface $(z = 0)$ of the beam from the linear and the nonlinear theories are exhibited in Fig. 7. The effect of the difference in the sign of the curvature in the left and the right halves of the beam is apparent in this plot for both the linear and the nonlinear theories. For $X_1 > 12$ cm, the deflection computed using the non-

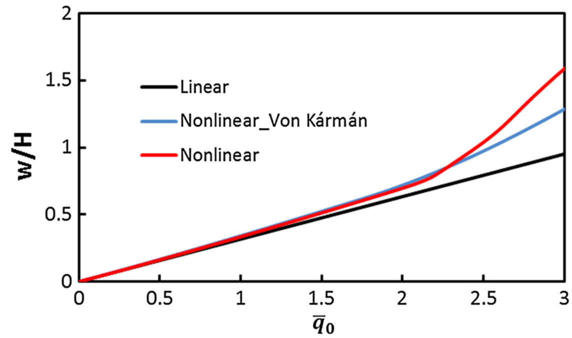

Fig. 6 For the linear and the nonlinear theories, variation of the non-dimensional deflection, $w(3\mathcal{L}/4, 0)/H$, versus the normalized pressure $\bar{q}_0$. The beam is loaded by a uniformly distributed pressure on the bottom surface (121 elements)

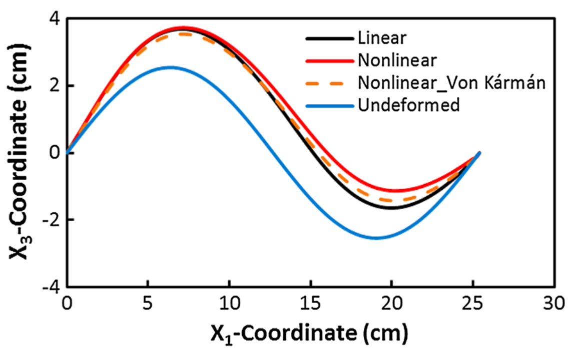

Fig. 7 For $\bar{q}_0 = 2.56$, deformed and undeformed positions of the beam centroidal axis computed using the linear and the nonlinear theories for the beam loaded by uniformly distributed pressure on the bottom surface of the beam, (121 elements)

linear theory is more than that from the linear theory. The distributions of the non-dimensional axial stress on the bottom surface of the beam from the linear and the nonlinear theories are compared in Fig. 8. Whereas for the linear theory the variation of σ_{xx} with respect to the arc length is symmetric about the midspan, that from the nonlinear theory is asymmetric. Also the value of σ_{xx} at the right edge is nearly 50 % more than that at the left edge. In Fig. 9 we have displayed through-the-thickness variation of the axial stress on the section $x = 3\mathcal{L}/4$ computed using the linear and the nonlinear theories. For all theories, $\sigma_{xx} = 0$ for $z/H = 0.15$. Thus the neutral surface defined by points where $\sigma_{xx} = 0$ does not coincide with beam's mid-surface.

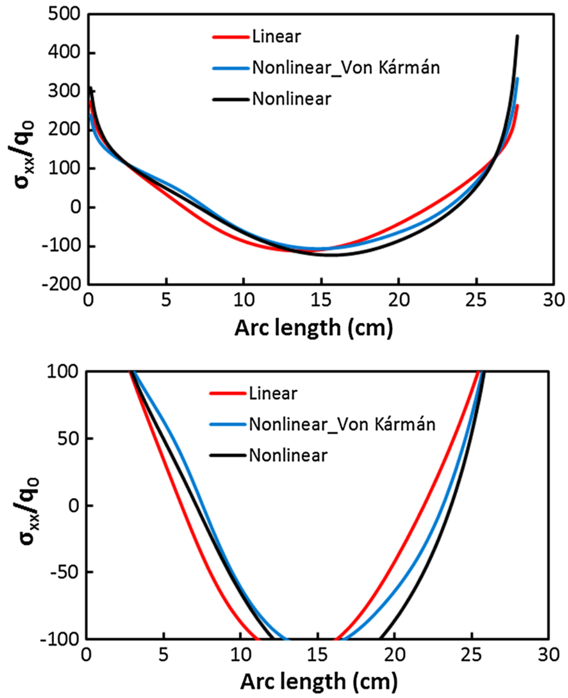

Fig. 8 For $\bar{q}_0 = 2.56$ and using the linear and the nonlinear beam theories, variation of the axial stress on the bottom surface, $z = -H/2$, (121 elements). The bottom Fig. is a magnified view of the stress distribution with the expanded vertical scale

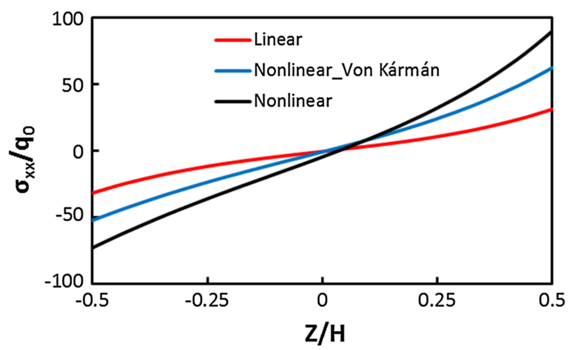

Fig. 9 Comparison of through-the-thickness variations of stress σ_{xx} at $x = 3\mathcal{L}/4$ computed using the linear and the nonlinear theories for the beam loaded by uniformly distributed pressure on the bottom surface of the beam, and the nondimensional pressure $\bar{q}_0 = 2.56$ (121 elements)

4 Conclusions

A third order shear and normal deformable theory (TSNDT) for analyzing finite deformations of a beam made of the St.Venant–Kirchhoff material has been developed. The theory has been used to analyze quasistatic deformations of a beam initially in the form of a full sine wave and loaded on the bottom surface by uniformly distributed tractions with $\theta = 0^\circ$, 30° and 90°. These values of θ imply that the applied load is either along the tangent to the surface, or inclined at 30° to the tangent or normal to the surface. Stresses are found from the displacement fields rather than through a post-processing technique. It is shown that traction boundary conditions on the bottom and the top surfaces of the beam are well satisfied. For $\theta = 90^\circ$, it is found that the axial stress at a point in the beam from the nonlinear theory is 4 times that from the linear theory, and the transverse deflection from the nonlinear theory is about 1.4 times that from the linear theory. For the linear theory, the maximum deflection at the midsection decreases with a decrease in the maximum radius of the beam.

Results for the von Kármán theory are generally between those for the linear and the nonlinear theories.

Acknowledgments This work was supported by the Office of Naval Research grant N00014-11-1-0594 to Virginia Polytechnic Institute and State University with Dr. Y. D. S. Rajapakse as the Program Manager. Views expressed in the paper are those of the authors and neither of the funding agency nor of authors' Institution.

References

1. Cosserat E, Cosserat F (1909) Théorie des Corps déformables. Paris, A. Hermann and Fils, vi+226 pp
2. Truesdell C (1960) The rational mechanics of flexible or elastic bodies 1638–1788. Venditioni Exponunt Orell Fussli, Turici
3. Timoshenko S (1921) On the correction of shear of the differential equation for transverse vibrations of prismatic bars. Philos Mag 41:744–746
4. Love AEH (1927) A treatise on the mathematical theory of elasticity. Cambridge University Press, Cambridge
5. Mindlin RD (1951) Influence of rotatory inertia and shear in fluxural motions of isotropic elastic plates. J Appl Mech 18:31–38
6. Reissner E (1945) The effect of transverse shear deformation on the bending of elastic plates. J Appl Mech 12:69–76
7. Ericksen JL, Truesdell C (1957/1958) Exact theory of stress and strain in rods and shells. Arch Ration Mech Anal 1:295–323
8. Antman SS (1976) Ordinary differential equation of non-linear elasticity.1. Foundations of theories of non-linearly elastic rods and shells. Arch Ration Mech Anal 61:307–351
9. Green AE, Naghdi PM (1974) Derivation of shell theories by direct approach. J Appl Mech 41:173–176
10. Chidamparam P, Leissa AW (1993) Vibrations of planar curved beams, rings, and arches. Appl Mech Rev 46:467–484
11. Hajiamaleki M, Qatu MS (2013) Vibrations of straight and composite beams: a review. Comp. Struc. 100:218–232
12. Carrera E, Petrolo M (2011) On the effectiveness of higher-order terms in refined beam theories, J Appl Mech 78, Art. No. 021013
13. Lo KH, Christensen RM, Wu EM (1977) A high-order theory of plate deformation—Part 1: Homogeneous plates. J Appl Mech 44:663
14. Vidoli S, Batra RC (2000) Derivation of plate and rod equations for a piezoelectric body from a mixed three-dimensional variational principle. J Elast 59:23–50
15. Batra RC, Vidoli S (2002) Higher-order piezoelectric plate theory derived from a three-dimensional variational principle. AIAA J 40:91–104
16. Batra RC, Vidoli S, Vestroni F (2002) Plane waves and modal analysis in higher-order shear and normal deformable plate theories. J Sound Vib 257:63–88
17. Allix O, Corigliano A (1999) Geometric and interfacial nonlinearities in the analysis of delamination in composites. Int J Solids Struct 25:1078–1105
18. Batra RC, Xiao J (2013) Finite deformations of curved laminated St. Venant-Kirchhoff beam using layer-wise third order shear and normal deformable beam theory (TSNDT). Compos Struct 97:147–164
19. Batra RC, Xiao J (2013) Analysis of post-buckling and delamination in laminated composite St Venant–Kirchhoff beams using CZM and layerwise TSNDT. Compos Struct 105:369–384
20. Xiao J, Batra RC (2014) Delamination in sandwich panels due to local water slamming loads. J Fluids Struct 48:122–155
21. Galvanett U, Pellegrino C, Schrefler BA (1998) A three-dimensional stress recovery procedure for composite materials. Comput Struct 69:567–575
22. Cho M, Kim KO, Kim MH (1996) Efficient higher-order shell theory for laminated composites. Compos Struct 34:197–212
23. Batra RC (2001) Comparison of Results from Four Linear Constitutive Relations in Isotropic Finite Elasticity. Int J Nonlinear Mech 36:421–432